Applied Surface Science 435 (2018) 476–482

Contents lists available at ScienceDirect

Applied Surface Science

journal homepage: www.elsevier.com/locate/apsusc

Full Length Article

Elastic, electronic and optical properties of the two-dimensional PtX_2 (X = S, Se, and Te) monolayer

Juan Du [a], Peng Song [b], Lizhen Fang [a], Tianxing Wang [a], Zhongming Wei [c], Jingbo Li [c], Congxin Xia [a,*]

[a] Department of Physics, Henan Normal University, Xinxiang, Henan 453007, China
[b] School of Physics, Nan Jing University, Nan Jing, Jiangsu 210093, China
[c] Institues of Semiconductors, Chinese Academy of Sciences, Beijing 100083, China

ARTICLE INFO

Article history:
Received 11 June 2017
Received in revised form 6 November 2017
Accepted 13 November 2017
Available online 14 November 2017

Keywords:
PtX_2 Monolayer
In-plane stiffness
Electronic structures

ABSTRACT

Through hybrid functional calculations, we study the elastic, electronic and optical properties of the two-dimensional (2D) PtX_2 (X = S, Se and Te) monolayer. The lattice constants increases and the band gap values decrease monotonously with increasing atomic number of chalcogenide elements. The tensile strain can reduce the band gaps and affect optical properties of 2D PtX_2 monolayers. Also, the indirect band structures are kept under considered strain range. Our results show that about −3% of compressive strain can induce semiconductor-to-metal transition. Moreover, the in-plane stiffness are 81 N/m for PtS_2, 64 N/m for $PtSe_2$, and 40 N/m for $PtTe_2$, which are smaller than that of 2D MoX_2 monolayers.

1. Introduction

In recent years, two-dimensional (2D) layered transition-metal dichalcogenides (TMDs) have been attracting significant attention due to their intriguing physical properties and potential applications in electronics and optoelectronics [1–6]. Unlike graphene, most of TMD_S monolayers have sizable band gaps in range of 1–3 eV [1,7–9], which paves the way to consider these materials for new-generation field nano-devices. For example, MoS_2 monolayer possesses a direct band gap of ~1.8 eV [10] and the mobility of about 200–500 $cm^2/V/s$, which makes it well suited for applications in transistors [2,11], and photo-detectors [2].

More recently, Wang et al. reported a newly synthesized $PtSe_2$ monolayer through the direct deposition of Se atoms on a Pt substrate [12], which has renewed interest in the 2D Pt-based chalcogenides [13,14]. It was shown by the photo-degradation experiment that $PtSe_2$ monolayer can serve as a visible light-driven photocatalyst. The Raman spectroscopy measurement on $PtSe_2$ found that the Raman active modes showed a clear intensity and position dependence with film thickness [15]. Li et al. found that the indirect band gaps of $PtSe_2$ monolayer can be tuned over a wide range via strain engineering [16]. Also, the strong electronic hybridization of interlayer S atoms make the few-layered PtS_2 to be a promising electronic material with tunable bandgap and relatively high mobility [17]. Manchanda et al predicted that hydrogenation may be an effective tool to introduce ferromagnetism in the 2D PtX_2 monolayer [18]. In addition, PtX_2 have been reported to be a good candidate for excellent thermoelectric application due to the very high Seebeck coefficients and strain can effectively tuned the thermoelectric properties [19,20]. Notably, the electron mobility of $PtSe_2$ and PtS_2 monolayer are even larger than that of black phosphorus (1000 $cm^2V^{-1}s^{-1}$) [21]. These properties make PtX_2 a potential candidate for novel applications in nanoelectronics, photocatalyst and optoelectronics.

However, further developments and applications of PtX_2 monolayer are restricted by the absence of a systematic research work on PtX_2 monolayer. The studies of some properties of PtX_2 monolayer, such as in-plane stiffness, are still not clear. In this work, through first-principles calculations, we systematically investigate the elastic, electronic and optical properties of the 2D PtX_2 monolayer.

2. Computational methods

All the calculations performed in this work are based on density functional theory method as implemented in the Vienna ab initio simulation package (VASP). The exchange–correlation functional is treated by the generalized gradient approximation (GGA) with the Perdew-Burke-Ernzerhofer (PBE) [22]. Because GGA underestimated the band gap [23], the hybrid functional Heyd-Scuseria-Ernzerhof (HSE06) [24,25] is also used for band structure

* Corresponding author.
E-mail address: xiacongxin@htu.edu.cn (C. Xia).

https://doi.org/10.1016/j.apsusc.2017.11.106
0169-4332/

calculations. Following the Monhkorst-Pack scheme [26], the Brillouin zone is sampled by a $15 \times 15 \times 1$ k-point mesh for the PBE and the $7 \times 7 \times 1$ k-point for the HSE06 calculations. Energy cutoff for plane-wave expansion is set to 500 eV. Meanwhile, to avoid any artificial interlayer interaction, a larger vacuum layer of 18 Å along z direction can be used for the 2D PtX_2 monolayer. All the structures are fully relaxed using the conjugated gradient method until the Hellmann-Feynman force on each atom was below 0.01 eV/Å.

3. Numerical results and discussions

3.1. Structural parameters and electronic structures of PtX_2 monolayer

We start briefly our calculations on the structural parameters and electronic structures of the PtX_2 monolayer structures with two X atoms and one Pt atom per unit cell, where it can be cleaved from the (0001) surface of the bulk PtX_2, as shown in Fig. 1. The optimized lattice constants can be seen in Table 1, which are very close to previous experiment and theory values [12,14,27]. We can see that the calculated values of Pt—X bond length are found in good agreement with other calculation results [14]. The values increase as X changes from S to Te due to the increasing atom size of S, Se, Te.

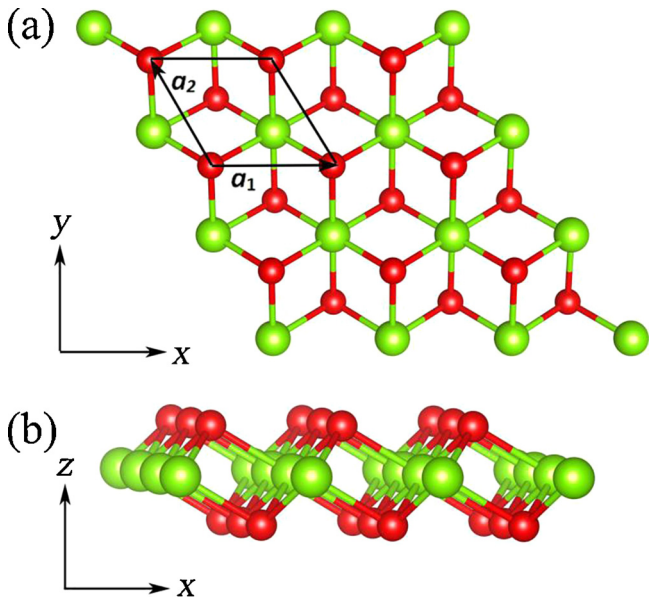

Fig. 1. (a) Top view and (b) side view of 2D PtX_2 monolayer. The green and red balls denote Pt and chalcogenide atoms, respectively. The rhombic regions present the unit cells.

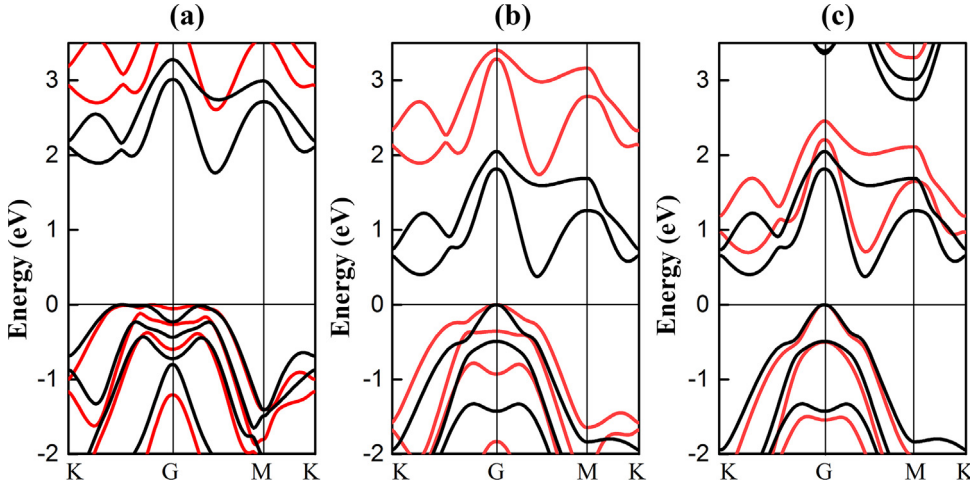

Fig. 2. Calculated band structures of (a) PtS_2 monolayer, (b) $PtSe_2$ monolayer, and (c) $PtTe_2$ monolayer. The fermi level is set at the VBM. Red and black lines are GGA-PBE + SOC and HSE06 + SOC calculated results.

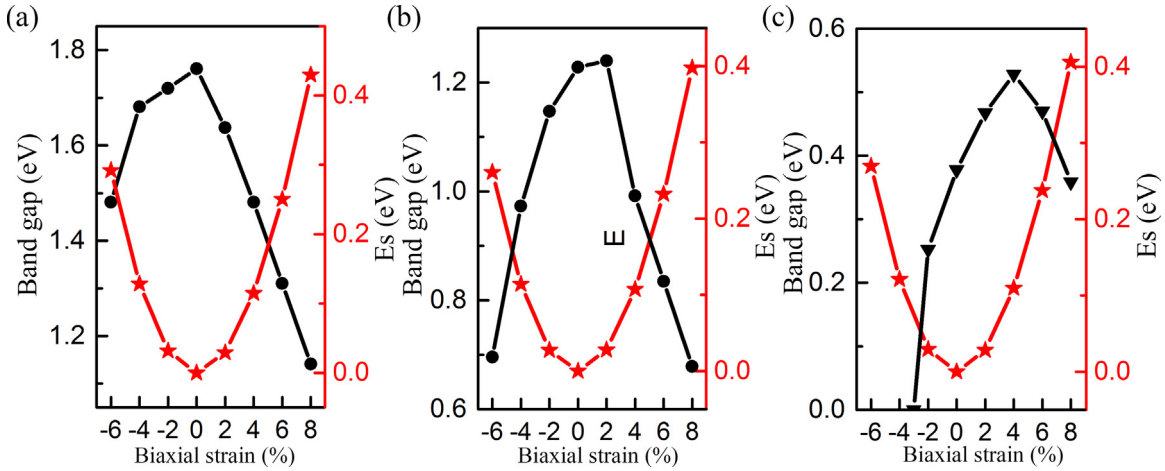

Fig. 3. The evolution of strain energy and band gap of (a) PtS_2, (b) $PtSe_2$ and (c) $PtTe_2$ monolayers under biaxial strain using GGA-PBE + SOC.

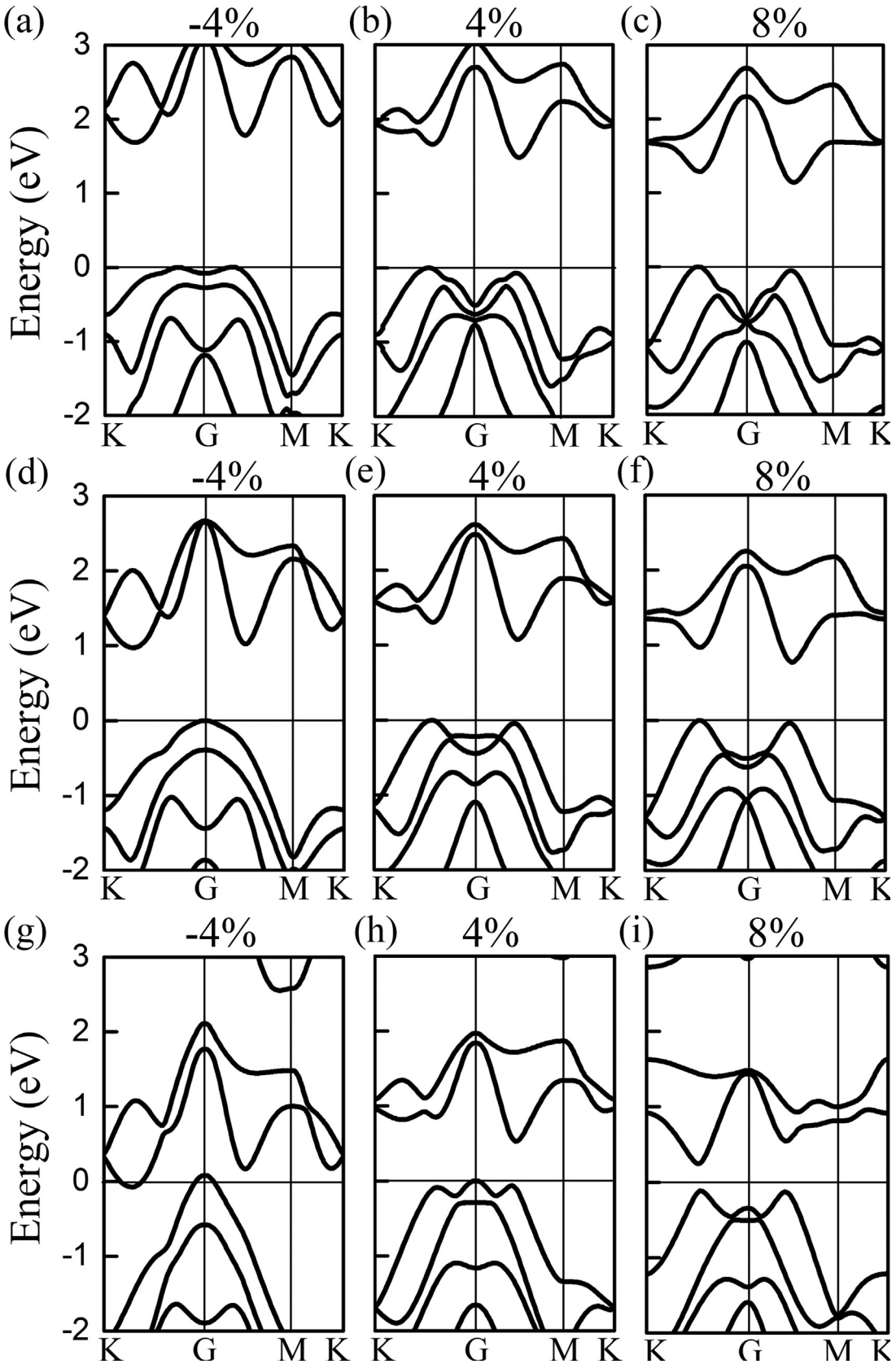

Fig. 4. Electronic band structure of (a) PtS_2, (b) $PtSe_2$, and (c) $PtTe_2$ monolayers corresponding to the applied biaxial strain −4%, 4% and 8%, respectively.

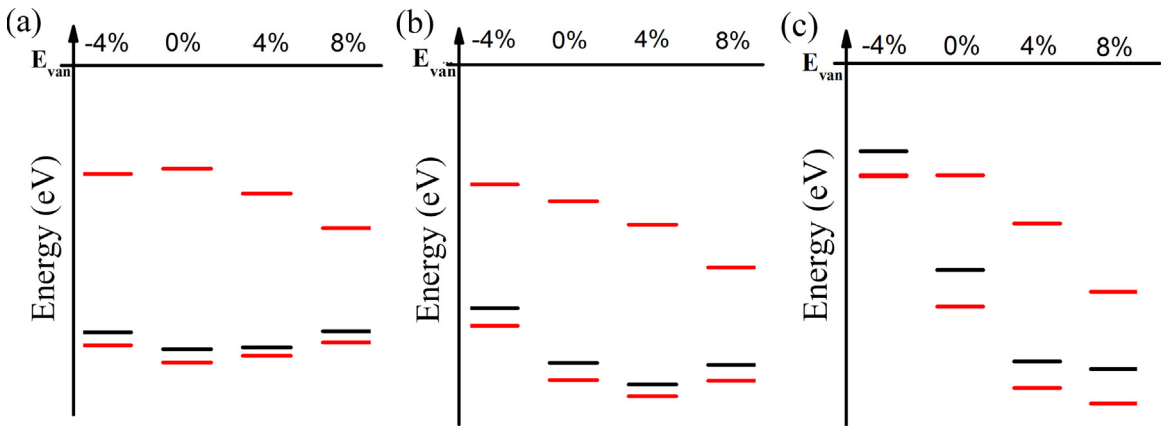

Fig. 5. The band alignment of (a) PtS_2 monolayer, (b) $PtSe_2$ monolayer, and (c) $PtTe_2$ monolayer with different strains. The horizontal red lines represent conduction band minimum (CBM) and the valence band maximum (VBM) of PtX_2 monolayer. The black crossed lines represent the Fermi level, and the E_{vac} stands for the vacuum level. All values were aligned with respect to the vacuum level.

Table 1
The structural parameters and elastic parameters of single-layer PtX_2 on GGA-PBE level. a and d are the distance between Pt atom and X (X = S, Se, Te) atom, respectively. t_1 and t_3 are the fitting parameters, ν and C are the Poisson' ratio and in-plane stiffness, respectively.

System	a (Å)	d (Å)	t_1	t_3	ν	C (N/m)
PtS_2	3.58	2.40	60.2	32.1	0.27	80.59
$PtSe_2$	3.75	2.53	52.2	26.3	0.25	64.35
$PtTe_2$	4.02	2.76	46.8	32.9	0.35	40.15

In order to understand the electronic characteristics of PtX_2 monolayer, in Fig. 2, we also present the band structures by using GGA-PBE + SOC and HSE06 + SOC calculations. It can be seen clearly from Fig. 2 that for the three PtX_2 monolayers, the conduction band minimum (CBM) and valence band maximum (VBM) lie in different high-symmetrical k-points, which indicates that all the PtS_2, $PtSe_2$ and $PtTe_2$ monolayer materials are semiconductors with indirect band gaps of 1.76 (2.61), 1.23 (1.73) and 0.38 (0.7) eV for GGA-PBE + SOC (HSE06 + SOC), respectively. Also, Fig. 2 shows that the general features of the band structures calculated by GGA-PBE + SOC and HSE06 + SOC are similar, except that the band gap calculated by HSE06 + SOC is larger than that by PBE + SOC method. This is because PBE usually underestimates the band gap values of semiconductor materials. Our results calculated by PBE and HSE06 are in great agreement with previous results [27,28].

3.2. Mechanical properties of PtX_2 monolayer

In addition, according to previous studies on mechanic properties of 2D semiconducting material, the related elastic properties can be represented by two parameters: in-plane stiffness C and Poisson's ratio ν. In order to calculate the elastic constants, the PtX_2 rectangular 1×2 supercell is considered. The in-plane stiffness is calculated as $C = (1/S_0)(\partial^2 E/\partial\varepsilon^2)$, where S_0 is the equilibrium area of the supercell, E is the total energy of the strained system and ε is for the uniaxial strain. Moreover, the Poisson's ratio is defined as$\nu = -\varepsilon_{trans}/\varepsilon_{axial}$, where ε_{trans} and ε_{trans} *and* ε_{axial} are the transverse and axial strains, respectively. In our calculations, the two lattice constants ε_a and ε_b change from −2% to 2% in an increment of 1%. We obtain 25 date points, and at each point the structure is fully re-optimized and the corresponding total energy is calculated. The calculated total energy can be written as $E_s = t_1\varepsilon_y^2 + t_2\varepsilon_x^2 + t_3\varepsilon_y\varepsilon_x$, in which E_s is the total strain energy per unit cell, defined as $E_s = E_{tot} - E_0$, where E_{tot} is the total energy of the strained unit cell, and E_0 is the total energy under equilibrium state. ε_a and ε_a are the strains along the x and y directions, respectively, and t_1–t_3 are related coefficients. It is found that t_1 is almost equal to t_2 due to isotropy in the honeycomb symmetry [29]. The in-plane stiffness and Poisson's ratio finally can be calculated using $C = (1/S_0)(2t_1 - t_3^2/2t_1)$ and $\nu = t_3/2t_1$. The related results are list in Table 1. It can be seen from Table 1 that the fitting parameters and as well as elastic constant C and ν. The in-plane stiffness C of PtS_2, $PtSe_2$ and $PtTe_2$ are 80.59, 64.35 and 40.15 N/m, respectively, which are relatively smaller than that of MoS_2 [30] and graphene [31], indicating that the former is less stiffer than the latter. Moreover, their Poisson's ratios are 0.27, 0.25 and 0.35, respectively. In order to testify the accuracy of our calculation, we also calculate values of C and ν by using the present method for ZrS_2 monolayer are 77 N/m and 0.20, which are in good accord with previous theoretical results [32]. In addition, it is clear that the in-plane stiffness degrades with increasing atomic number of chalcogenide atoms. As we know, the electronegativity is the scale of the ability of an atom to attract electrons in a compound. The greater the electronegativity of the element, the stronger the ability of its atoms to attract electrons in the compound. The electronegativity decreases as we go down the periodic table, from S to Te, which results in a weaker interaction between the Pt and X atoms. Thus, the in-plane stiffness of PtX_2 decreases when X goes from S to Te. The trend of the in-plane stiffness is similar as that of 2D GaX (X = S, Se, Te) monolayer from S to Te [33].

3.3. Tunable band gap under uniform strain

It is well known that strain technology is widely employed in modulating the electronic properties of semiconductors. Here, we systematically investigate electronic properties of the PtX_2 monolayer considering strain effects. Numerical results in Fig. 3 show that whether tensile or compressive strain, the strain energy increases monotonically with the increases of strain within the loaded range, demonstrating the deformation of PtX_2 monolayer is elastic. In addition, the harmonic approximation is well preserved under the strain $-0.02 \leqq \varepsilon_{xy} \leqq 0.02$, and beyond this value, the E_s-ε curve becomes inharmonic because the contributions of higher order terms are not negligible.

The variation of the band gaps of PtX_2 monolayer calculated by GGA-PBE + SOC as a function of strain is summarized in Fig. 3. In the case of tensile strain, the gap value first increases, and then decreases linearly with increasing of tensile strain. While for compress strain, the bandgap monotonically decreases. In contract, the variation of PtX_2 monolayer under compress strain does not exhibit linear feature, mainly due to the CBM transfers among several high symmetry, which can be seen in Fig. 4. Most interestingly, the band

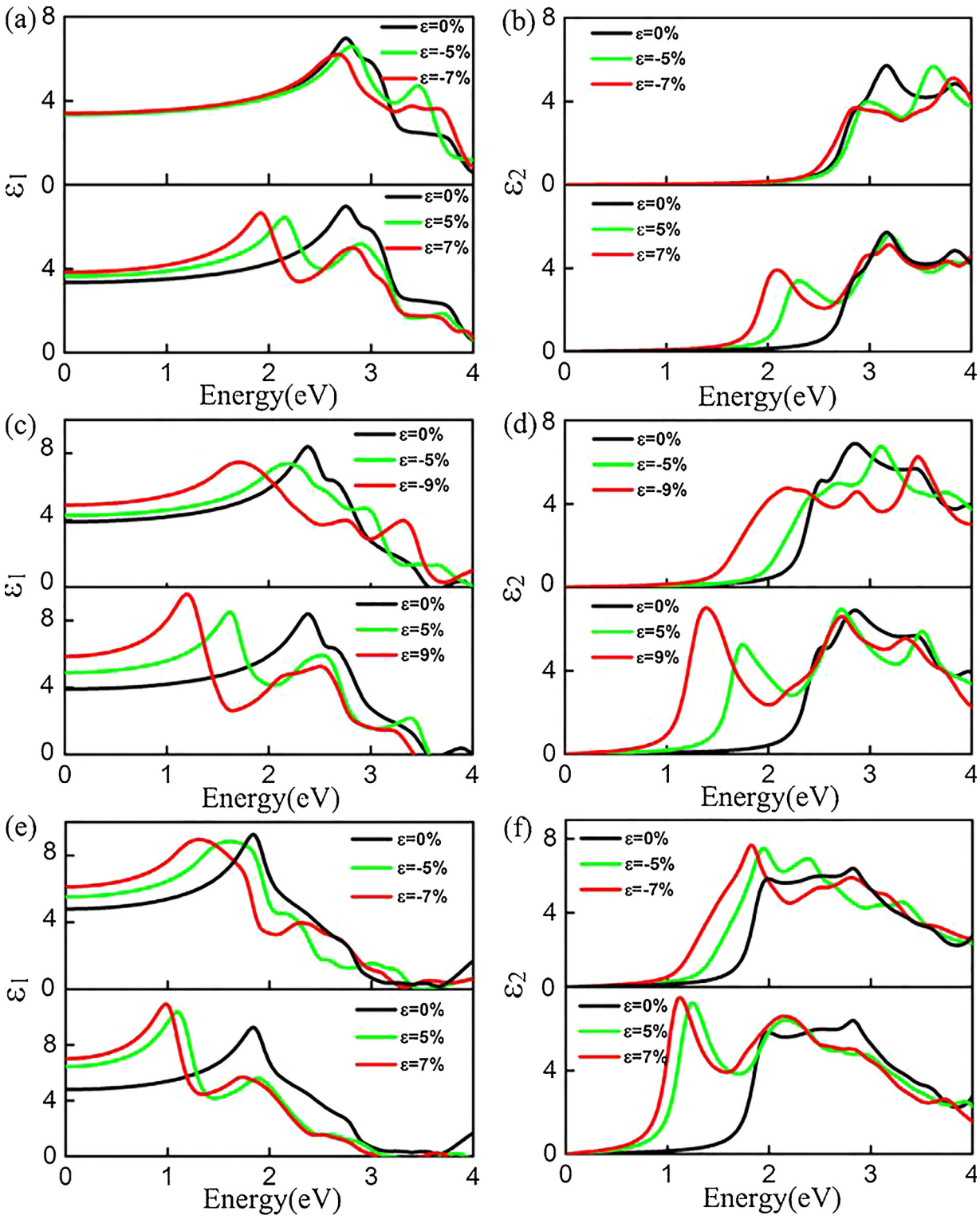

Fig. 6. The real part ε_1 and the image part ε_2 of the dielectric function of the (a,b) PtS_2 monolayer, (c,d) $PtSe_2$ monolayer and (e,f) $PtTe_2$ monolayer, corresponding to the applied biaxial strain 5%, 7%, 9% and −5%, −7%, −9%, along the x-y plane.

gap of $PtTe_2$ monolayer reduced to zero after the compress strain reached 3%, as shown in Fig. 3, which is in good agreement with the works of Guo et al [34], indicating our calculation is correct. All the results testify that the band bap of the PtX_2 monolayer can be modified over a wide range, which opens up new opportunities for their applications in nanoelectronic devices.

In order to understand the mechanism of the band gap change under the influences of applied strain, in Fig. 4, we calculate the band structures of PtX_2 with applied different strains by using the PBE + SOC. For compressive strain from 0%–8%, the VBM located at Γ has not been changed. While the CBM gradually moves from the middle between Γ and M to the middle between G and K. However, for tensile strain, the VBM of PtX_2 monolayer is found to move

from Γ to X with slow upward shift, while the CBM at the middle between Γ and M remain unchanged with biaxial tensile strain. However, for the $PtTe_2$ monolayer in the case of 8% tensile strain, Fig. 4 shows that it is a direct band gap semiconductor because the CBM and VBM lie at the middle between K and Γ points. Moreover, the spin-orbit splitting at Γ point of PtX_2 monolayer monotonically decreases with the increasing strain from −6% to 8%. To further analyze the electronic characteristics of PtX_2 monolayer with 4%, 8% and −4% strain, the band alignments are also calculated, as shown in Fig. 5. We can find that for the PtS_2 monolayer, tensile and compressive strains can result in lowering the CBM while shifting upward the VBM. For $PtSe_2$ monolayer, increasing tensile strain can induce the VBM first decreases and then increases, and the CBM increases; while compressive strain can increase the levels of CBM and VBM. On the other hand, for $PtTe_2$ monolayer, the levels of VBM and VBM decrease with increasing strain. Thus, it can be seen that the electronic structures of PtX_2 monolayer show similar behavior mainly due to the same atomic configuration and spatial symmetry group.

3.4. Optical properties

The frequency-dependent dielectric function$\varepsilon(\omega)$is a complex quantity dealing with the most important aspect of optical properties. The $\varepsilon(\omega)$can be expressed as $\varepsilon(\omega) = \varepsilon_1(\omega) + i\varepsilon_2(\omega)$. The imaginary part $\varepsilon_2(\omega)$ of the dielectric function could be calculated from the momentum matrix elements between the occupied and unoccupied wave functions.

$$\varepsilon_2(w) = \frac{4\pi^2 e^2}{m^2 w^2} \sum_{nn'} \int \left| P_{nn'}(k) \right|^2 \frac{dS_k}{\nabla w_{nn'}(k)} \quad (1)$$

The real part $\varepsilon_1(w)$ of the dielectric function can be derived from the imaginary part $\varepsilon_2(w)$ using the Kramers-Kronig relations.

$$\varepsilon_1(\omega) = 1 + \frac{2}{\pi} p \sum_{nn'} \int \frac{w' \varepsilon_2\left(w'\right)}{w'^2 - w^2} dw' \quad (2)$$

In Fig. 6, we present the imaginary part$\varepsilon_2(\omega)$dispersion of PtX_2 monolayer along in-plane light polarization direction, considering different strain values. The results show that the threshold energy values decrease with increasing strain, which is due to the results of the decrease of the band gap of PtX_2 monolayer. Moreover, the threshold energy decreases obviously with the increase of tensile strain at higher magnitude of strain. However, when the PtX_2 monolayer is applied by the compression strain, the threshold energy decreases in a smaller magnitude than tensile strain. The trends are exactly consistent with the band gap variation in Fig. 2. On the application of all the studied strain, the structure peak is found to be red shifted towards lower energy as shown in Fig. 6. Thus, strain can affect obviously the optical transitions and optical properties of 2D PtX_2 monolayer.

In order to understand clearly the real part$\varepsilon_1(\omega)$of the dielectric function of PtX_2 monolayer, Fig. 6 presents the real parts$\varepsilon_1(\omega)$as a function of photon energy in the PtX_2 monolayer, considering different strain values. It is clear from Fig. 6(a, c, e) that the real parts$\varepsilon_1(\omega)$of dielectric function are zero at certain photon energy, and then decreases to negative value with increasing photon energy. In addition, Fig. 6 also shows that the values of the static dielectric constants$\varepsilon_1(0)$are increased when strain is increased in the PtX_2 monolayer. The trends are exactly opposite to the change of band gap in Fig. 2. It can be understood within the framework of Penn model expression for semiconductors, $\varepsilon_1(0) \approx 1 + \left(\hbar w_p / E_g\right)^2$ in which static dielectric constant is inversely proportional to the band gap.

4. Conclusions

In summary, through first-principles calculations, we have studied the elastic, electronic and optical properties of the PtX_2 monolayer. The studies find that the 2D PtS_2, $PtSe_2$ and $PtTe_2$ monolayers show similar elastic, electronic and optical properties because they share the same atomic configuration and spatial symmetry group. The in-plane stiffness degrades gradually with increasing atomic number of chalcogenide atoms, which are less stiffer than MoS_2. Upon applying the tensile strain, the gap value decreases approximately linearly. While the variation of band gaps under compressive strain does not exhibit linear feature. The structure peak of strained PtX_2 monolayer is found to be red shifted towards lower energy in the optical absorption edge, which makes it a compelling candidate for optoelectronic devices. Moreover, the ability to modulate the band gap of PtX_2 monolayer over an appreciable range of biaxial strain opens up new opportunities for their applications in nanoelectronic devices.

Acknowledgments

This research was supported by the National Natural Science Foundation of China under Grant Nos. 11674084 and 11674310. And Natural Science Foundation of Henan under Grant No. 162300410169. The calculations are also supported by The High Performance Computing Center of Henan Normal University.

References

[1] Q.H. Wang, K. Kalantar-Zadeh, A. Kis, J.N. Coleman, M.S. Strano, Electronics and optoelectronics of two-dimensional transition metal dichalcogenides, Nat. Nanotechnol. 7 (2012) 699–712.
[2] B. Radisavljevic, A. Radenovic, J. Brivio, V. Giacometti, A. Kis, Single-layer MoS_2 transistors, Nat. Nanotechnol. 6 (2011) 147–150.
[3] Y.J. Zhang, J.T. Ye, Y. Matsuhashi, Y. Iwasa, Ambipolar MoS_2 thin flake transistors, Nano Lett. 12 (2012) 1136–1140.
[4] H. Li, Z.Y. Yin, Q.Y. He, H. Li, X. Huang, G. Lu, D.W.H. Fam, A.I.Y. Tok, Q. Zhang, H. Zhang, Fabrication of single and multilayer MoS_2 film-based field-effect transistors for sensing NO at room temperature, Small 8 (2012) 63–67.
[5] Z.Y. Yin, H. Li, H. Li, L. Jiang, Y.M. Shi, Y.H. Sun, G. Lu, Q. Zhang, X. Chen, H. Zhang, Single-layer MoS_2 phototransistors, ACS Nano 6 (2012) 74–80.
[6] S. Jo, N. Ubrig, H. Berger, A.B. Kuzmenko, A.F. Morpurgo, Mono-and bilayer WS_2 light-emitting transistors, Nano Lett. 14 (2014) 2019–2025.
[7] N. Zibouche, P. Philipsen, A. Kuc, T. Heine, Transition-metal dichalcogenide bilayers: switching materials for spintronic and valleytronic applications, Phys. Rev. B 90 (2014) 125440.
[8] J.A. Wilson, A.D. Yoffe, The transition metal dichalcogenides discussion and interpretation of the observed optical, electrical and structural properties, Adv. Phys. 18 (1969) 193–335.
[9] H.L. Zhuang, R.G. Hennig, Computational search for single-layer transition-metal dichalcogenide photocatalysts, J. Phys. Chem. C 117 (2013) 20440–20445.
[10] K.F. Mak, C. Lee, J. Hone, J. Shan, T.F. Heinz, Atomically thin MoS_2: a new direct-gap semiconductor, Phys. Rev. Lett. 105 (2010), 136805.
[11] G.H. Lee, Y.J. Yu, X. Cui, N. Petrone, C.H. Lee, M.S. Choi, D.Y. Lee, C. Lee, W.J. Yoo, K. Watanabe, T. Taniguchi, C. Nuckolls, P. Kim, J. Hone, Flexible and transparent MoS_2field-effect transistors on hexagonal boron nitride-graphene heterostructures, ACS Nano 7 (2013) 7931–7936.
[12] Y. Wang, L. Li, W. Yao, S. Song, J.T. Sun, J. Pan, X. Ren, C. Li, E. Okunishi, Y.Q. Wang, E. Wang, Y. Shao, Y.Y. Zhang, H.T. Yang, E.F. Schwier, H. Iwasawa, K. Shimada, M. Taniguchi, Z. Cheng, S. Zhou, S. Du, S.J. Pennycook, S.T. Pantelides, H.J. Gao, Monolayer $PtSe_2$, a new semiconducting transition-metal-dichalcogenide, epitaxially grown by direct selenization of Pt, Nano Lett. 15 (2015) 4013–4018.
[13] X. Chia, A. Adriano, P. Lazar, Z. Sofer, J. Luxa, M. Pumera, Electrocatalysis of layered group 5 metallic transition metal dichalcogenides (MX_2, M=V, Nb, and Ta; X=S, Se, and Te), Adv. Funct. Mater. 26 (2016) 4306–4318.
[14] M.J. Piotrowski, R.K. Nomiyama, J.L.F.D. Silva, Role of van der waals corrections for the PtX2 (X=O, S, Se) compounds, Phys. Rev. B 88 (2013) 075421.
[15] C. Yim, K. Lee, N. McEvoy, M.O. Brien, S. Riazimehr, N.C. Berner, C.P. Cullen, J. Kotakoski, J.C. Meyer, M.C. Lemme, G.S. Duesberg, High-performance hybrid electronic devices from layered $PtSe_2$films grown at low temperature, ACS Nano 10 (2016) 9550–9558.
[16] P.F. Li, L. Li, X.C. Zeng, Tuning the electronic properties of monolayer and bilayer $PtSe_2$ via strain engineering, J. Mater. Chem. C 4 (2016) 3106–3112.

[17] Y.D. Zhao, J.S. Qiao, P. Yu, Z.X. Hu, Z.Y. Lin, S.P. Lau, Z. Liu, W. Ji, Y. Chai, Extraordinarily strong interlayer interaction in 2D layered PtS_2, Adv. Mater. 28 (2016) 2399–2407.
[18] P. Manchanda, A. Enders, D.J. Sellmyer, R. Skomski, Hydrogen-induced ferromagnetism in two-dimensional Pt dichalcogenides, Phys. Rev. B 94 (2016) 104426.
[19] S.D. Guo, J.L. Wang, Spin-orbital coupling effect on the power factor in semiconducting transition-metal dichalcogenide monolayers, Semicond. Sci. Technol. 31 (2016) 095011.
[20] S.D. Guo, L. Zhang, Biaxial strain tuned thermoelectric properties in monolayer $PtSe_2$, J. Mater. Chem. C 4 (2016) 9366–9374.
[21] Z.S. Huang, W.X. Zhang, W.L. Zhang, Computational search for two-dimensional MX_2 semiconductors with possible high electron mobility at room temperature, Materials 9 (2016) 716–728.
[22] J.P. Perdew, K. Burkeand, M. Ernzerhof, Electronic structure calculations of solids using the WIEN2k package for material sciences, Phys. Rev. Lett. 77 (1996) 3865–3868.
[23] H. Xiao, J. Tahir-Kheli, W.A. Goddard, Accurate band gaps for semiconductors from density functional theory, J. Phys. Chem. Lett. 2 (2011) 212–217.
[24] J. Heyd, G.E. Scuseria, M. Ernzerhof, Hybrid functionals based on a screened coulomb potential, J. Chem. Phys. 118 (2003) 8207–8215.
[25] J. Heyd, G.E. Scuseria, M. Ernzerhof, Erratum: “hybrid functionals based on a screened coulomb potential”, J. Chem. Phys. 124 (2006), 219906.
[26] H.J. Monkhorst, J.D. Pack, Special points for Brillouin-zone integrations, Phys. Rev. B 13 (1976) 5188–5192.
[27] H.L. Zhuang, R.G. Hennig, Computational search for single-layer transition-metal dichalcogenide photocatalysts, J. Phys. Chem. C 117 (2013) 20440–20445.
[28] F.A. Rasmussen, K.S. Thygesen, Computational 2D materials database: electronic structure of transition-metal dichalcogenides and oxides, J. Phys. Chem. C 119 (2015) 13169–13183.
[29] L.D. Landau, L.P. Pitaevskii, E.M. Lifshitz, A.M. Kosevich, Theory of Elasticity, Vol. 7, third edition, 1986.
[30] Q. Yue, J. Kang, Z.Z. Shao, X.A. Zhang, S.L. Chang, G. Wang, S.Q. Qin, J.B. Li, Mechanical and electronic properties of monolayer MoS2 under elastic strain, Phys. Lett. A 376 (2012) 1166–1170.
[31] M. Topsakal, S. Cahangirov, S. Ciraci, The response of mechanical and electronic properties of graphane to the elastic strain, Appl. Phys. Lett. 96 (2010), 091912.
[32] Y. Li, J. Kang, J.B. Li, Indirect-to-direct band gap transition of the ZrS_2 monolayer by strain: first-principles calculations, RSC Adv. 4 (2014) 7396–7401.
[33] L. Huang, Z.H. Chen, J.B. Li, Effects of strain on band gap and effective mass in two-dimensional monolayer GaX (X=S, Se, Te), RSC Adv. 5 (2015) 5788–5794.
[34] S.D. Guo, J.L. Wang, Small compressive strain induced semiconductor-metal transition and tensile strain enhanced thermoelectric properties in monolayer $PtTe_2$, Semicond. Sci. Technol. 32 (2017) 055004.